

Self-Regulating Solar Steam Generators Enable Volatile Organic Compound Removal through In Situ H_2O_2 Generation

Shuai Zhou,[#] Ruihua He,[#] Jianchuan Pei, Weiping Liu, Zhaohong Huang, Xiaogang Liu, and Juan Wang*



Cite This: *Environ. Sci. Technol.* 2022, 56, 10474–10482



Read Online

ACCESS |



Metrics & More



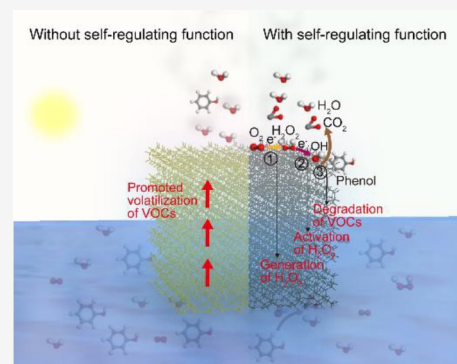
Article Recommendations



Supporting Information

ABSTRACT: Interfacial solar steam generation for clean water production suffers from volatile organic compound (VOC) contamination during solar-to-steam conversion. Here, we present a solar steam generator based on the integration of melamine foam (MF), polydopamine (PDA), and Ag/AgCl particles. Together with the high photothermal conversion efficiency (ca. 87.8%, 1 kW/m²) achieved by the PDA thin film, the Ag/AgCl particles can efficiently activate the localized generation of H_2O_2 and $\bullet OH$ in situ, thus degrading the VOCs during the rapid vapor generation. The generation of H_2O_2 and $\bullet OH$ in situ also facilitates the creation of a buffer zone containing H_2O_2 and $\bullet OH$ for the rapid removal of organic pollutants in the surrounding water attracted to the solar vapor generator, demonstrating a self-cleaning steam generator toward various volatile compounds such as phenol, aniline, 2,4-dichlorophenol, and *N,N*-dimethylformamide in a wide range of concentrations.

KEYWORDS: interfacial water purification, photocatalysis, in situ generation of H_2O_2 , Fenton-like reaction, volatile organic compounds



1. INTRODUCTION

With the rapid human civilization, population growth, and development of industry and agriculture, the supply of clean water is becoming increasingly important, especially through green and sustainable technologies.^{1–6} Recently, solar interfacial water vapor conversion with high energy conversion efficiency and low environmental impact has emerged as a promising water purification technique for clean water supply in portable devices or water-scarce rural areas hindered by technical or financial conditions.^{7–11} Materials with broad absorption bands, including carbon-based materials, metal/semiconductor nanomaterials, and polymers, have been widely adopted for water vapor interface systems.^{12–17} However, a limitation of current approaches is that volatile organic contaminants (VOCs, synthetic or natural organics) in wastewater are always collected along with water steam during evaporation because of their low boiling point, resulting in the accumulation of VOCs in the collected water.^{18–21}

Recently, the construction of a selective solution diffusion path has been demonstrated as an efficient strategy to physically hinder the diffusion of VOCs together with vapor.^{19,20} However, the VOCs would be accumulated and stored with increased concentration in the source water.²⁰ Degradation of VOCs in situ during the interfacial evaporation process becomes a more promising strategy.^{21–25} One method to address this problem is to utilize Fenton/Fenton-like water remediation processes with interfacial solar vapor generation to degrade VOCs in situ during evaporation.^{21–23} In this regard, Fe-based Fenton/Fenton-like catalysts, such as $CuFeMnO_4$ and ferrocene-based metal–organic frameworks (MOFs), have

been employed to activate hydrogen peroxide (H_2O_2) to produce hydroxyl radicals ($\bullet OH$) for the mineralization of VOCs at interfacial solar evaporators.^{21,23} However, these systems always require regular replenishment of H_2O_2 , which may incur additional manufacturing and storage costs. Moreover, the uncontrollable rapid activation of H_2O_2 can lead to excess $\bullet OH$, which can disappear rapidly, because of its short lifetime ($\sim 1 \mu s$).²⁶ In recent years, photocatalytic in situ synthesis of H_2O_2 has been widely explored with the development of various catalysts including g- C_3N_4 -based composites,^{27–30} as well as efficient in situ generation and photo-assisted activation of H_2O_2 to $\bullet OH$ for the treatment of organic pollutants.^{31,32} Thus, the development of single devices that can achieve simultaneous photothermal water evaporation together with a photodriven in situ generation and activation of H_2O_2 – $\bullet OH$ may become an efficient strategy to remove the VOCs during the interfacial evaporation process, which still remains a challenge.

Herein, we demonstrate an interfacial solar evaporator based on PDA and Ag/AgCl comodified melamine foam (MF), which is capable of simultaneously evaporating and purifying VOC-contaminated wastewater without the need for exoge-

Received: March 24, 2022

Revised: June 14, 2022

Accepted: June 15, 2022

Published: June 28, 2022



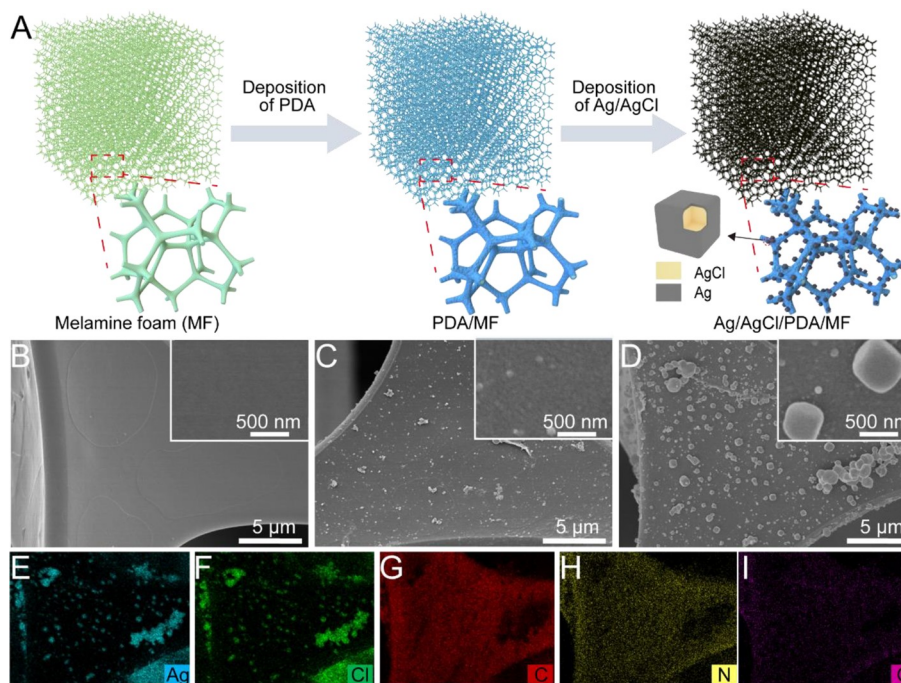


Figure 1. (A) Schematic of the preparation of Ag/AgCl/PDA/MF. (B–D) SEM images of MF, PDA/MF, and Ag/AgCl/PDA/MF, respectively. (E–I) Corresponding EDX elemental mapping of Ag, Cl, C, N, and O, respectively. Insets in (B–D) are the corresponding high-resolution images of the samples.

nous H_2O_2 . In our design, PDA-loaded MF is applied to effectively transport water and convert it to steam via the process of solar energy conversion. Ag/AgCl particles are employed as photocatalysts to enable the localized generation of H_2O_2 and $\bullet\text{OH}$ under light irradiation. We found that the introduction of Ag/AgCl significantly decreased the concentrations of various VOCs such as phenol, aniline, 2,4-dichlorophenol, and *N,N*-dimethylformamide in the collected water by catalyzing the photoinduced Fenton-like reaction in the degradation of these compounds. As an added benefit, the localized generation of H_2O_2 by Ag/AgCl provides an H_2O_2 – $\bullet\text{OH}$ buffer zone that enables the prevention and self-purification of organic contaminants in the solar steam generator.

2. EXPERIMENTAL SECTION

2.1. Preparation of PDA/MF. The PDA/MF device was prepared with the following steps. First, tri(hydroxymethyl) amino-methane hydrochloride (50×10^{-3} M), dopamine hydrochloride (8×10^{-3} M), copper sulfate (2×10^{-3} M), and hydrogen peroxide (50×10^{-3} M) were added into and mixed well with 20 mL of deionized water. MF was cut into a cube with a size of $2 \times 2 \times 2$ cm³ and then immersed into the above solution at room temperature for 6 h to facilitate the polymerization of dopamine and deposition of PDA nanoparticles on the structure network of MF.³³ The obtained product cubic foam in dark gray was denoted as PDA/MF. The prepared samples including the samples synthesized below were washed with deionized water, dried at 80 °C in a vacuum oven for 8 h, and stored for further experiment.

2.2. Preparation of Ag/AgCl/PDA/MF. For the preparation of Ag/AgCl/PDA/MF, the obtained PDA/MF through the above procedure was first soaked into 1.5 mM silver nitrate aqueous solution for 2 min and 1.5 mM sodium chloride solution for another 2 min. This process was repeated 20 times,

followed by irradiation under UV light (365 nm, 2.5 mW/m²) for 2 h to accelerate the formation of Ag/AgCl.³⁴

2.3. Measurement of Water Evaporation Performance. The device was supported by a 5 mm thick polystyrene foam and placed on the water surface under the irradiation of a solar simulator. The indoor experiments were conducted at ~24 °C and ~55% relative humidity (RH). A solar simulator (Aulight, CEL-AA550) outputting AM 1.5G spectrum was used as the light source. The solar flux was adjusted by changing the current and calibrated using an optical power meter (Aulight, CEL-NP2000-2). The mass change of different devices was recorded every 2 min using a laboratory balance (Mettler Toledo, ME204E) with an accuracy of 0.1 mg after light irradiation of 15 min, except the evaporation rates in the dark.

2.4. Measurement of Water Purification Performance. Phenol, aniline, 2,4-dichlorophenol, and *N,N*-dimethylformamide were selected as the treated VOCs, and the experiment was performed. Feed water with VOCs was prepared freshly before use and sealed to avoid releasing of VOCs to air. The set was covered using an acrylic collector and irradiated under solar light (simulated or natural one) for 8 h. The collected condensed water was collected for subsequent residual VOC measurement.

2.5. Set Up of the Continuous Eight-Day Experiment. To conduct the eight-day continuous experiment, the feed water (phenol solution) was replaced with fresh prepared one every day. A certain amount of condensed water and feed water was fetched for residual VOC measurement every 2 h.

2.6. Set Up of the Continuous Eight-Day Water Treatment with a Continuous Flow. The phenol solution stored in a sealed plastic box was continuously pumped into the bottom of the solar evaporation set as feed water and pumped out to a sealed container box on the right side, both at a rate of 2.5 mL/min. After every 8 h irradiation, the

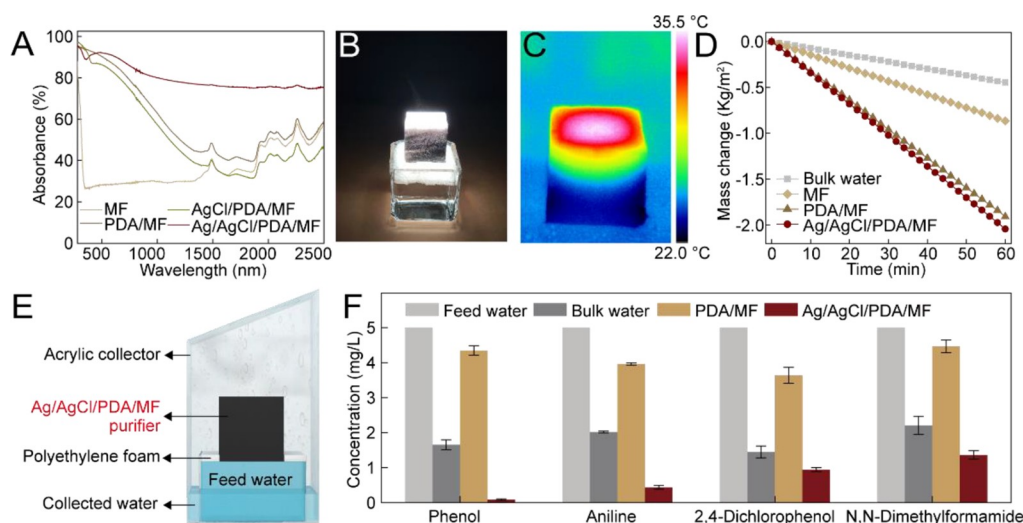


Figure 2. (A) UV-vis-NIR absorption spectra of MF, PDA/MF, AgCl/PDA/MF, and Ag/AgCl/PDA/MF toward the full solar spectrum. (B) Photograph of the interfacial evaporation device under simulated solar irradiation (1 kW/m^2). (C) Infrared thermal image of Ag/AgCl/PDA/MF on the water surface, under simulated solar irradiation (1 kW/m^2). (D) Mass change in different systems under simulated solar irradiation (1 kW/m^2). (E) Schematic of the solar-powered interfacial water purification system. (F) Measured concentrations of volatile organic compounds in the feed water and collected vapor for different systems under simulated solar irradiation (1 kW/m^2). It should be noted that the concentration of each volatile organic compound is 5 mg/L .

condensed water was fetched for subsequent residual VOC measurement.

3. RESULTS AND DISCUSSION

3.1. Sample Fabrication and Catalytic Performance Measurement. Figure 1A is a schematic diagram showing the procedure used to prepare the interfacial solar steam generator. A commercial MF was selected as the building substrate for the generator because it has a porous network and a smooth surface (Figure S1). MF was cut into a $2 \text{ cm} \times 2 \text{ cm} \times 2 \text{ cm}$ cube and then coated with PDA. PDA-coated MF (PDA/MF) was then deposited with AgCl particles by successively dipping the foam in silver nitrate and sodium chloride solutions and repeating several times. Subsequently, the as-prepared sample was treated with UV irradiation at 365 nm for 2 h to facilitate the reduction of AgCl to Ag to form an Ag/AgCl/PDA/MF composite.³⁴

Figure 1B–D show representative scanning electron micrographs of MF, PDA/MF, and Ag/AgCl/PDA/MF samples, respectively. These images show the formation of regular particles ($\sim 500 \text{ nm}$) on MF surfaces after PDA and Ag/AgCl modifications. Figure 1E–I show the corresponding element mapping of the Ag/AgCl/PDA/MF composite. Regular particles in the image contain only Ag and Cl, while C, N, and O are evenly distributed throughout the MF skeleton. X-ray diffraction (XRD) characterization shows that both Ag and AgCl phases have formed in the sample (Figure S2).³⁵ The high-resolution transmission electron microscopy images (Figure S3) show that the clear lattices are consistent with the (200) and (111) planes of AgCl and Ag, respectively, which matched well with the XRD results of the Ag/AgCl/PDA/MF sample.³⁴ This further suggests that the regular particles on MF are Ag/AgCl hybrids.

Ultraviolet-visible-near-infrared (UV-vis-NIR) absorption spectra of the as-prepared solar vapor generators show that loading PDA on MF (PDA/MF) significantly increased the absorption efficiency for light in the visible spectral range (Figure 2A) because PDA can absorb visible light efficiently.³³

After the deposition of Ag/AgCl particles on the foam, the absorption capacity for the full solar spectrum was boosted, especially for light in the NIR range. This phenomenon may be due to the formation of Ag metal, which absorbs NIR light because of plasmonic dipole resonance.³⁶ This strong absorption capacity ($\sim 80.6\%$) of the set at the dry state may endow the system with excellent performance in converting sunlight into vapor.¹²

The solar energy conversion capacity of the Ag/AgCl/PDA/MF composite was then validated under irradiation at 1 kW/m^2 using a solar simulator (Figure 2B). We observed that the Ag/AgCl/PDA/MF composite generated a maximum surface temperature ($35.5 \text{ }^\circ\text{C}$) higher than those of pristine MF ($27.1 \text{ }^\circ\text{C}$) or PDA/MF ($32.5 \text{ }^\circ\text{C}$) (Figures 2C and S6). At the same solar irradiance, Ag/AgCl/PDA/MF exhibited the highest vapor generation rate ($2.04 \text{ kg/m}^2/\text{h}$) compared with that of PDA/MF or MF alone (Figure 2D).

To elucidate the VOC removal ability of Ag/AgCl-modified PDA/MF evaporators, we intentionally added a series of VOCs (5 mg/L), including phenol, aniline, 2,4-dichlorophenol, and *N,N*-dimethylformamide, to the feed water and measured the residue concentration of the aforementioned organic molecules in the collected water after vapor condensation (Figure 2E). The collected water production rates of Ag/AgCl/PDA/MF were approximately 0.55 , 0.86 , and $1.16 \text{ kg/m}^2/\text{h}$ under 1 , 1.5 , and 2 kW/m^2 irradiation, respectively (Figure S9). The PDA/MF steam generator had high VOC residues in the collected water, with concentrations exceeding 3 mg/L for all VOCs (Figure 2F). Despite the relatively low VOC residues (~ 1.45 – 2.21 mg/L), the steam generation rate for direct collection from bulk water evaporation is approximately 4.6 times slower than that achievable using solar interfacial steam generators. In stark contrast, the vapor collected by Ag/AgCl/PDA/MF has a much lower VOC content. We measured a residue phenol concentration of 0.08 mg/L , indicating 98% phenol removal in the condensed water. Notably, the interfacial solar steam generators also displayed considerable removal performance for aniline, 2,4-dichlorophenol, and *N,N*-dimethylformamide,

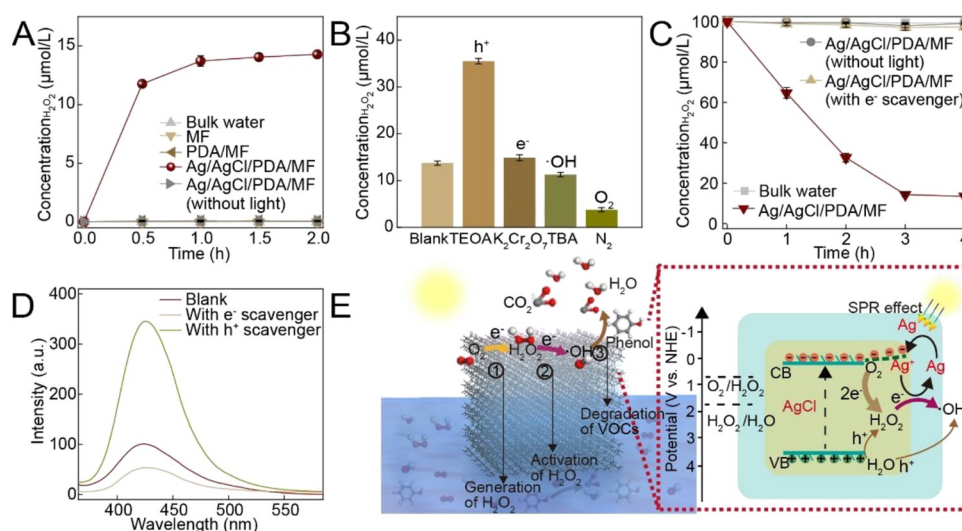


Figure 3. (A) Concentration of H_2O_2 produced in solutions using different devices with and without light irradiation. (B) Concentration of H_2O_2 produced by Ag/AgCl/PDA/MF with different situations under light irradiation for 1 h. (C) Change of H_2O_2 concentration in the presence of Ag/AgCl/PDA/MF under different conditions, with an initial H_2O_2 concentration of $100 \mu\text{mol/L}$. (D) Fluorescence detection of the $\bullet\text{OH}$ radical with terephthalic acid as the fluorescent probe, with the addition of different scavengers. The measurements were conducted after simulated solar irradiation (1 kW/m^2) for 0.5 h. (E) Schematic of the scavenging process of VOCs in the device with in situ self-regulating $\text{H}_2\text{O}_2 \rightarrow \bullet\text{OH}$ conversion function.

with 91, 81, and 73% removal, respectively. The varied VOC removal efficiency may be attributed to the difference on the organic compound structure, which affects greatly the reaction rate constant of $\bullet\text{OH}$ with the organic compounds.³⁷

3.2. Catalytic Mechanism Investigation. We next investigated in detail the possible mechanism of Ag/AgCl/PDA/MF for VOC removal. First, we tested the direct adsorption of VOCs by immersing the devices in a VOC solution and keeping them at dark for 1 h to reach the adsorption equilibrium (Figure S10). The slight difference between the two concentrations before and after the adsorption process indicates a negligible contribution of adsorption to the removal of VOCs. Therefore, we suggest that catalytic degradation plays a dominant role in this process. The feed water and condensed vapor (collected water) were analyzed via liquid chromatography–mass spectrometry (LC–MS) (Figure S11). Under solar irradiation (1 kW/m^2), there was a tiny amount of phenol detected in the condensed vapor (collected water), which manifests the excellent removal capability of our Ag/AgCl/PDA/MF system. The feed water was also analyzed via LC–MS. It can be seen that, with the increased reaction time (8 h), the phenol concentration in feed water decreased rapidly, with the detection of a small amount of succinic acid, salicylic acid, tartaric acid, and maleic acid, which suggest the efficient degradation of phenol (Figure S11B). A prolonged reaction time to 16 h showed a further removal of almost all the organic compounds, suggesting the excellent photocatalytic degradation capability of our set (Figure S11C).

We next carried out a set of experiments to understand the underlying chemical processes for VOC removal by Ag/AgCl/PDA/MF. Without the addition of organic compounds, we observed efficient H_2O_2 generation attributable to Ag/AgCl/PDA/MF alone, with a maximum generation capacity of $\sim 15 \mu\text{mol/L}$ ($280 \mu\text{mol/L/g}$ per catalyst) in aqueous solution under 1 sun irradiation (1 kW/m^2) for 1.5 h (Figure 3A). We found that the pristine MF and PDA/MF produced no H_2O_2 under the same conditions, suggesting that Ag/AgCl is

responsible for the production of H_2O_2 . One reason for the efficient photogeneration and degradation of H_2O_2 by Ag/AgCl/PDA/MF is the effective production of photogenerated carriers (both e^- and h^+ pairs) by the device. This was evidenced by the observation of a strong photocurrent in Ag/AgCl/PDA/MF, with a current density of over $1 \mu\text{A/cm}^2$ under 1 sun irradiation (Figure S12A).

The quenching experiments were further performed to investigate the catalytic mechanism associated with the generation of H_2O_2 under light irradiation, as shown in Figure 3B. It can be seen that O_2 participated in the formation of H_2O_2 as we observed a sharp decline in H_2O_2 concentration when we irradiated a solution purged with nitrogen. The addition of triethanolamine (TEOA, a typical h^+ scavenger) significantly promoted H_2O_2 production, in comparison with the original system. We attribute this to the increased electron concentration because the trapping of h^+ not only can show the role of e^- but also contribute to the release of more electrons via hindering the recombination of photogenerated electrons and holes. Taking into consideration the phenomenon that the presence of O_2 affects the H_2O_2 generation greatly, we can propose that reduction of O_2 by electrons may play important role for the production of H_2O_2 .²⁷ Additionally, the presence of $\text{K}_2\text{Cr}_2\text{O}_7$ (a typical e^- scavenger, with a reaction kinetic constant $\sim 0.635 \text{ min}^{-1}$ for e^-)³⁸ also resulted in a slightly higher H_2O_2 production rate than that of the original system. This phenomenon indicated that the oxidation of H_2O via holes also contribute to the formation of H_2O_2 , and the consumption of e^- in the solution can contribute to more released holes for the reaction. Based on the above phenomenon and analysis, we propose that the H_2O_2 production mainly follows the two reactions below.^{27,39,40}

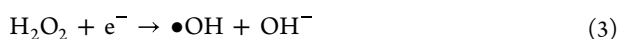


Because we observed no significant changes in the H_2O_2 concentration when the $\bullet\text{OH}$ scavenger TBA was added to the

reaction, this suggests that the formation of H_2O_2 does not consume $\bullet\text{OH}$ in the system.

On the other hand, we found that Ag/AgCl/PDA/MF can catalyze the photodegradation of H_2O_2 . In an H_2O_2 solution with an initial concentration of $100 \mu\text{mol/L}$ (~ 7 -fold higher than the maximum photogeneration capacity of H_2O_2 by Ag/AgCl), the presence of Ag/AgCl/PDA/MF and 1 sun irradiation decreased the concentration of H_2O_2 by $\sim 90\%$ within 3 h (Figure 3C). Interestingly, we found that H_2O_2 was not decomposed under dark conditions. This indicates that Ag/AgCl/PDA/MF undergoes a photo-Fenton reaction pathway to decompose H_2O_2 . It was confirmed that the photogenerated electrons are mainly responsible for the activation of H_2O_2 because the concentration of H_2O_2 hardly changed when $\text{K}_2\text{Cr}_2\text{O}_7$ (electron scavenger) was added to an H_2O_2 solution with an initial concentration of $100 \mu\text{mol/L}$ (Figure 3C). The subsequent electron spin resonance (ESR) analysis in Figure S13A unveiled the existence of $\bullet\text{OH}$ radicals during the photogeneration/degradation of H_2O_2 , while $\bullet\text{O}_2^-$ and $^1\text{O}_2$ were not detectable (Figure S13B). This implies that the VOC removal by the system is mainly attributed to the photogenerated H_2O_2 and $\bullet\text{OH}$ radicals.

We further monitored the $\bullet\text{OH}$ concentration in the system with terephthalic acid as the fluorescent probe.⁴¹ As indicated by Figure 3D, the addition of a h^+ scavenger (TEOA) resulted in significantly promoted generation of $\bullet\text{OH}$, suggesting the dominant role of e^- for $\bullet\text{OH}$ generation. However, when e^- was quenched, the signal intensity obviously decreased but still showed a slight generation of $\bullet\text{OH}$. Therefore, it is suggested that the oxidation of H_2O by h^+ may also contribute to a small portion of $\bullet\text{OH}$ generation, but the activation of H_2O_2 contributed dominantly to the generation $\bullet\text{OH}$, following the equation below:^{31,32}



3.3. Identification on the Role of Ag/AgCl. To identify the role of Ag/AgCl played in the generation and activation of H_2O_2 to $\bullet\text{OH}$, sets of experiment were performed next. Because Ag on the Ag/AgCl/PDA/MF sample was formed by the reduction of AgCl under UV light irradiation, we propose that under light irradiation, the following Ag/Ag⁺ cycled reactions occur to maintain stable Ag/AgCl:



X-ray photoelectron spectroscopy (XPS) and XRD analysis of the catalysts before and after the experiment (Figure S14A and B) showed a stable material composition after the experiment, which may also manifest the stably cycled Ag/AgCl redox process above.

We next performed optical measurement and plotted the band gap structure of AgCl derived from Mott–Schottky analysis (Figure S12B and C, see the SI for detailed information). As shown in Figure 3E, potentials of the conduction band (CB) and valence band (VB) of AgCl on the PDA/MF substrate were calculated as 0.26 and 3.55 V (vs NHE), respectively. Because the reduction potential of $\text{O}_2/\text{H}_2\text{O}_2$ is more positive than the CB potential and the oxidation potential of $\text{H}_2\text{O}_2/\text{H}_2\text{O}$ is higher than the VB potential of

AgCl, the photogenerated e^- and h^+ on AgCl theoretically can catalyze the formation of H_2O_2 by either reducing O_2 or oxidizing H_2O , which is matching well with the experiment phenomenon and analysis performed above. Additionally, the VB position of AgCl also satisfies the potential requirement for h^+ to oxidize H_2O to $\bullet\text{OH}$, matching well with the observed tiny generation of $\bullet\text{OH}$ under the presence of h^+ .

To better understand the respective role of Ag and AgCl for the H_2O_2 generation and activation, we further synthesized Ag/AgCl and AgCl powders according to the similar procedure adopted for our device fabrication, respectively, to exclude the possible interference of PDA on the absorption spectra. The Ag/AgCl showed absorption toward light in the UV and visible range, while AgCl only absorbed UV light (Figure S15), which indicates that the absorption of visible light in Ag/AgCl was contributed by Ag. We also prepared the Ag/PDA/MF sample via coating Ag particles on PDA/MF to obtain Ag/PDA/MF as a control sample (see the SI for detailed information).

Subsequently, the performance of Ag/PDA/MF and Ag/AgCl/PDA/MF under the irradiation of a selective light wavelength was measured. Under respective UV ($< 365 \text{ nm}$) and visible ($\sim 400\text{--}800 \text{ nm}$) irradiation, Ag/PDA/MF did not present any activity either to the generation of H_2O_2 or its activation, which indicates that Ag cannot work solely. Under the same condition, Ag/AgCl/PDA/MF showed activities toward both generation and activation of H_2O_2 (Figure S16). Because AgCl cannot absorb visible light, the activity presented by Ag/AgCl/PDA/MF under visible light irradiation may attribute to the plasmonic-generated electrons on Ag, which was transferred to AgCl rapidly and subsequently. The activity of AgCl toward H_2O_2 generation and activation under UV light irradiation matched well with the above band gap discussion that the electrons generated on AgCl can contribute to the generation and activation of H_2O_2 simultaneously.

Taking together the relevant investigation and discussion above, the overall mechanism of Ag/AgCl for the generation and activation of H_2O_2 can be summarized as follows. First, under solar light irradiation, the electrons generated on Ag will transfer to AgCl and work together with the electrons generated by AgCl itself to reduce oxygen to H_2O_2 . The separated holes on AgCl also contribute partially to the H_2O_2 formation, via oxidation of H_2O . The in situ activation of H_2O_2 to $\bullet\text{OH}$ happened simultaneously on the catalyst surface, with the assistance of electrons generated on AgCl, as well as the electrons transferred from Ag to AgCl. The holes generated on AgCl also contributed to the formation of $\bullet\text{OH}$, via oxidation of water, in a certain degree. Besides, the Ag/Ag⁺ redox cycle may also contribute to the photocatalytic activation of H_2O_2 to $\bullet\text{OH}$, as reported by the literature.^{41,42} A schematic diagram for the entire process on the solar interfacial system was proposed, as shown in Figure 3E.

To identify the main reaction sites on the foam sample, we measured the transmittance of the Ag/AgCl/PDA/MF sample in different thickness n ($n = 0.5, 1.0, \text{ and } 2.0 \text{ cm}$). As shown in Figure S17, Ag/AgCl/PDA/MF $n = 0.5$ still showed a certain transmittance of light. However, no penetration of the light was observed for samples with larger thickness. Therefore, we propose that H_2O_2 generation and activation into $\bullet\text{OH}$ occur at the foam surface with a certain depth, where we can receive light, and subsequently diffuse to the bottom section because of the concentration difference.

3.4. Performance Comparison with the Conventional Set. To further investigate the performance of our device, we

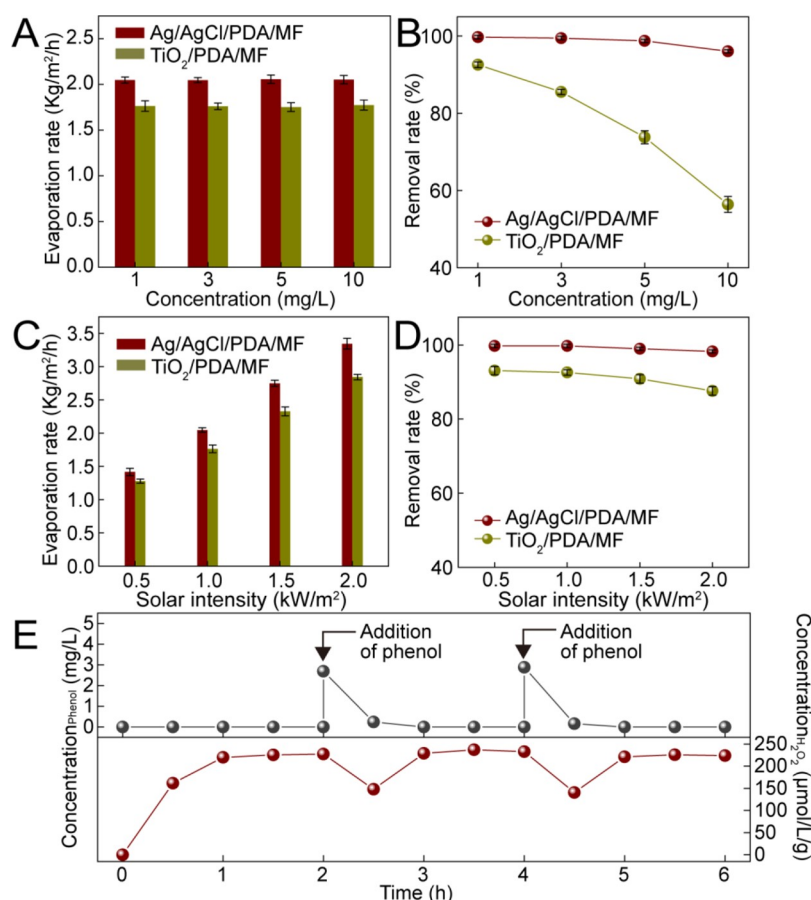


Figure 4. (A) Evaporation performance and (B) phenol removal rate of Ag/AgCl/PDA/MF and TiO₂/PDA/MF with different phenol concentrations under simulated solar irradiation (1 kW/m²). (C) Evaporation performance and (D) phenol removal rate of Ag/AgCl/PDA/MF and TiO₂/PDA/MF under simulated solar irradiation at different light intensities. The phenol concentration of phenol was set at 1 mg/L. (E) Measured H₂O₂ and phenol concentrations over time using Ag/AgCl particles under simulated solar irradiation (1 kW/m²).

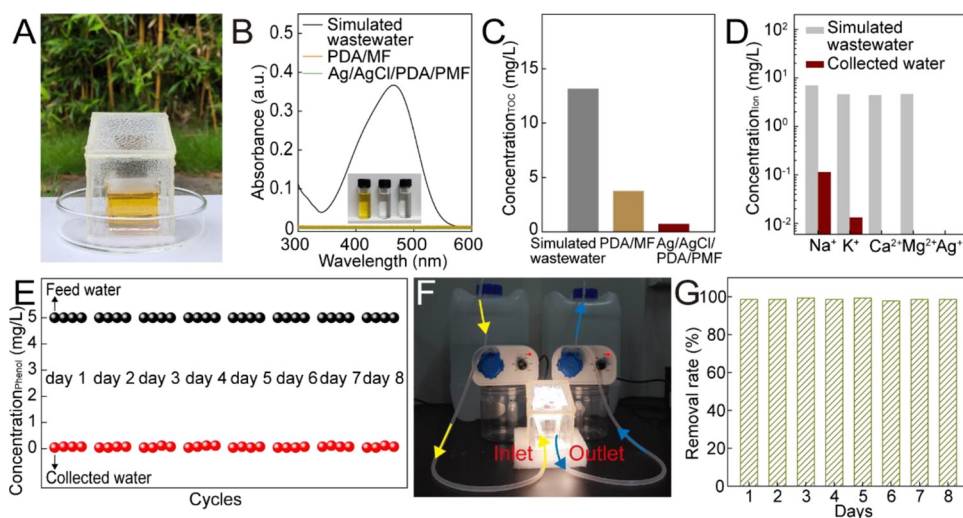


Figure 5. (A) Photograph of the solar-powered interfacial water purification system under outdoor sunlight. (B) UV-vis absorption spectra of simulated wastewater and collected water vapor from different systems. Inset in (B) shows the photograph of the simulated wastewater (left) and collected water vapor from PDA/MF (middle) and Ag/AgCl/PDA/PMF (right) systems. (C) TOC concentration of the simulated wastewater and collected water vapor from different systems. (D) Measurement of metal ion concentrations in the simulated wastewater and collected water vapor from the Ag/AgCl/PDA/MF system. (E) Phenol concentration of the feed water and collected water vapor during a continuous experiment, with the Ag/AgCl/PDA/MF system for water purification at a solar intensity of 1 kW/m². It should be noted that the phenol solution (5 mg/L) was adopted as feed water. (F) Photograph of the solar-powered interfacial water purification system with continuous water feeding. (G) Phenol removal rate of the collected water vapor during a continuous experiment with the Ag/AgCl/PDA/MF system under simulated solar irradiation (1 kW/m²).

compared the VOC removal of Ag/AgCl/PDA/MF and TiO₂/PDA/MF under various conditions. TiO₂ is a photocatalyst applied to the direct removal of VOCs in several interfacial solar steam generators, but it does not generate H₂O₂.^{24,25} In a typical experiment, we added phenol to the feed water at different concentrations (1, 3, 5, and 10 mg/L) (Figure 4A, B). Our solar steam generator showed stable phenol removal rates of over 95% at all tested VOC concentrations. In stark contrast, the removal efficiency of TiO₂/PDA/MF dropped sharply to ~60% when the phenol concentration was increased to 10 mg/L.

The stability of the two devices under tuned solar irradiation from 0.5 to 2 kW/m² was tested next (Figure 4C, D). The Ag/AgCl/PDA/MF always showed high stable phenol removal efficiency of almost 100%. It should be mentioned that the Ag/AgCl/PDA/MF device always showed excellent water evaporation performance, with a vapor generation rate of over 2 kg/m²/h in all the above experiments. At the fastest water evaporation rate of over 3 kg/m²/h (under 2 kW/m² irradiation), the Ag/AgCl/PDA/MF still exhibited a phenol removal efficiency of nearly 100%, while the phenol removal rate of TiO₂/PDA/MF decreased by ~5%. These results unambiguously indicate the superiority of our system in the efficient removal of VOCs and rapid water evaporation compared to the state-of-the-art techniques (Table S1).

A dynamic monitoring of H₂O₂ concentration in the feed water with the periodic addition of phenol showed that the H₂O₂ concentration increased rapidly and reached an equilibrium state after about 2 h (Figure 4E). The addition of phenol (3 mg/L) after 2 h of reaction resulted in a rapid decrease in the concentrations of H₂O₂ and phenol. After 3 h of reaction, the phenol concentration decreased to almost zero and the H₂O₂ concentration increased back to its original value. A similar situation can be repeated with the addition of phenol after 4 h of reaction. This phenomenon can be attributed to the consumption of •OH by the phenol, which can force the further activation of H₂O₂. Once phenol was completely oxidized, H₂O₂ will be restored as a buffer zone in the system for further use. The above experiment has demonstrated that organic contaminants in the system are self-cleaning because of the H₂O₂ buffer with excellent stability.

3.5. Investigation of Potential for Practical Use. To investigate the potential of the device for practical application, we conducted an outdoor water purification experiment using river water from Qizhen Lake, Zijiang campus of Zhejiang University. In the experiment, artificial wastewater was first prepared by adding phenol and methyl orange to the sampled river water, which act as volatile and nonvolatile organic compounds (5 mg/L). After 4 h of continuous outdoor sunlight exposure (Figure S19B), the condensed vapor was collected using a portable setup (Figure 5A). After water evaporation and condensation, the characteristic absorption peak of methyl orange was no longer observed in the collected water (Figure 5B) and the color of the solutions changed from orange (simulated wastewater) to colorless (collected water) (inset in Figure 5B), indicating efficient removal of methyl orange. The total organic carbon (TOC) of the water sample decreased significantly from 13.1 to 0.7 mg/L in the collected vapor of Ag/AgCl/PDA/MF (Figure 5C). Ions in the effluent before and after treatment were analyzed by inductively coupled plasma mass spectrometry (ICP-MS) (Figure 5D). The metal ions, including Na⁺, Mg²⁺, K⁺ and Ca²⁺, were almost

undetectable compared with the artificial wastewater (Figure 5E). The absence of Ag⁺ in the collected water suggests the high stability of the Ag/AgCl/PDF/MF composite system. Both the detected TOCs and the salinity of the collected water were far below the China standard for drinking water quality (GB5749-2006), revealing the potential of our design for effective water treatment.^{25,43}

The stability of our solar steam generator was further evaluated in an eight-day continuous experiment with a phenol solution (5 mg/L), under simulated solar irradiation (1 kW/m²). To simulate real conditions, the system was subjected to 8 h of irradiation each day and rested for the remaining 16 h. The feed water was replaced every day. The condensed steam and feed water were taken every 2 h for analysis. The collected water showed stable and efficient removal of phenol (over 98%) during the eight-day continuous experiment (Figure 5E). Besides the stability against VOCs removal, the evaporation rate of the generator during the continuous experiment also did not show any obvious change (Figure S19C), suggesting the excellent stable performance of our system. The silver ion concentration in the feed water before and after the continuous experiment was analyzed via ICP-MS (Figure S14C). There was only around 4.95 μg/L detected in the feed water after experiments, which is approximately 0.0025% of the original loading amount of Ag/AgCl on the system, suggesting good stability of the composites.

We next performed a similar eight-day continuous water treatment experiment (8 h per day) with a continuous flow of feed water containing phenol. As shown in Figure 5F, the phenol solution was continuously pumped into the bottom of the solar evaporation set as feed water and pumped out to the container on the right side, at a rate of 2.5 mL/min. As indicated by Figure 5G, the daily collected water showed a stable removal of phenol. Moreover, the solar purifier showed stable evaporation and phenol removal performance toward Wahaha pure water, tap water, as well as river water sample fetched from Qizhen lake of Zhejiang university (Figure S20). The VOC treatment performance of Ag/AgCl/PDA/MF toward water at different pHs was conducted, and the results are plotted in Figure S19D. It can be seen that our set exhibits a high phenol removal efficiency (~98%) toward the pH range from 1 to 11. The removal efficiency slightly decreased to around 81% at pH 13, which is possibly due to the consumption of •OH by OH⁻ at high pH values.^{44,45} All these experiments indicate the excellent potential of our set for the treatment of organic pollutants.

4. ENVIRONMENTAL IMPLICATIONS

Interfacial solar steam generation is one of the promising strategies to alleviate global water shortage, and research of the system has primarily focused on improving the water evaporation efficiency; however, from the water treatment perspective, the coexistence of organic pollutants in water would evaporate out together with vapor, especially the volatile compounds, which would hinder its broader application. In this work, we have demonstrated a self-cleaning solar steam generator by combining interfacial photothermal evaporation with in situ photogeneration and activation of H₂O₂ to •OH radicals. Therefore, this rational design enables the Ag/AgCl/PDA/MF steam generator to simultaneously remove VOCs and distill water under various conditions. As measured, the solar purifier showed efficient removal of VOCs such as phenol with efficiency over 98%. Under tuned solar irradiation from

0.5 to 2 kW/m², our system always showed high stable phenol removal efficiency over 95%. There are some previous reports that demonstrated that direct photocatalytic generation of •OH may also remove phenol efficiently. However, in comparison with the direct generation of •OH radicals in photocatalytic reactions, the H₂O₂ generated in our system can be stored stably in the solution, in comparison with the short lifetime of •OH radicals. Therefore, the localized generation of H₂O₂ can sustainably provide a buffer zone containing H₂O₂, which ensures the prevention and self-purification of organic contaminants in the generator. In particular, this interfacial solar purifier presents efficient treatment of VOCs in a wide pH range from 1 to 13, good VOCs treatment stability toward different water sources (including Wahaha pure water, tap water, and river water), as well as excellent stability during a continuous eight-day experiment, all of which suggest great potential of our system for practical use. Although novel mental Ag was involved in the device fabrication, the usage amount of Ag is quite low, and the leaching of Ag to the water source is limited in a safe range. To this regard, we believe that our results not only present a strategy to efficiently treat VOCs in water during the solar interfacial evaporation process but may also inspire the environmental treatment technology based on the heterogeneous catalysis process, especially for an advanced oxidation process with exogenous H₂O₂. Also, this design may also serve as a rising strategy for portable wastewater treatment. Also, from the perspective of a similar system design with high efficiency, because the respective capture of electrons and holes in our reaction system both resulted in boosted H₂O₂ production rates, although in different degrees, this may inspire us that solutions to increase the separation of electron–hole pairs also play a dominant role for the system design with good performance.

■ ASSOCIATED CONTENT

SI Supporting Information

The Supporting Information is available free of charge at <https://pubs.acs.org/doi/10.1021/acs.est.2c02067>.

Additional method details, SEM images, XRD patterns, HRTEM images, FT-IR spectra, UV–vis–NIR absorption and transmittance spectra, infrared thermal images, solar-to-steam efficiency, adsorption experiments, liquid chromatography, photocurrent response measurement, Mott–Schottky measurement, ESR spectra, XPS spectra, real-time recording of outdoor solar intensities, and evaporation and photocatalytic performance at different conditions (PDF)

■ AUTHOR INFORMATION

Corresponding Author

Juan Wang – Institute of Environmental Health, MOE Key Laboratory of Environmental Remediation and Ecosystem Health, College of Environmental & Resource Sciences, Zhejiang University, Hangzhou 310058, China; orcid.org/0000-0002-1340-9011; Email: wjuan@zju.edu.cn

Authors

Shuai Zhou – Institute of Environmental Health, MOE Key Laboratory of Environmental Remediation and Ecosystem Health, College of Environmental & Resource Sciences, Zhejiang University, Hangzhou 310058, China

Ruihua He – Department of Chemistry, National University of Singapore, Singapore 117549, Singapore

Jianchuan Pei – College of Environment and Resources, Zhejiang A&F University, Hangzhou 311300, China

Weiping Liu – Institute of Environmental Health, MOE Key Laboratory of Environmental Remediation and Ecosystem Health, College of Environmental & Resource Sciences, Zhejiang University, Hangzhou 310058, China; orcid.org/0000-0002-1173-892X

Zhaohong Huang – Singapore Institute of Manufacturing Technology, Singapore 138634, Singapore

Xiaogang Liu – Department of Chemistry, National University of Singapore, Singapore 117549, Singapore; orcid.org/0000-0003-2517-5790

Complete contact information is available at:

<https://pubs.acs.org/10.1021/acs.est.2c02067>

Author Contributions

#S.Z. and R.H. contributed equally to this study.

Notes

The authors declare no competing financial interest.

■ ACKNOWLEDGMENTS

We thank funding support provided from the National Natural Science Foundation of China (No. 22176170 and 21976152), the Natural Science Foundation of Zhejiang Province, China (No. LR21B070002), the GSK-EDB Trust Fund Program through SIMTech (R-143-000-698-504), and the Open Research Program of Key Laboratory of 3D Micro/Nano Fabrication and Characterization of Zhejiang Province, Westlake University.

■ REFERENCES

- (1) Zhao, F.; Guo, Y.; Zhou, X.; Shi, W.; Yu, G. Materials for solar-powered water evaporation. *Nat. Rev. Mater.* **2020**, *5*, 388–401.
- (2) Wang, Z. X.; Horseman, T.; Straub, A. P.; Yip, N. Y.; Li, D. Y.; Elimelech, M.; Lin, S. H. Pathways and challenges for efficient solar-thermal desalination. *Sci. Adv.* **2019**, *5*, No. eaax0763.
- (3) Li, Z.; Xu, X.; Sheng, X.; Lin, P.; Tang, J.; Pan, L.; Kaneti, Y. V.; Yang, T.; Yamauchi, Y. Solar-powered sustainable water production: state-of-the-art technologies for sunlight-energy-water nexus. *ACS Nano* **2021**, *15*, 12535–12566.
- (4) Li, H.; Yan, Z.; Li, Y.; Hong, W. Latest development in salt removal from solar-driven interfacial saline water evaporators: advanced strategies and challenges. *Water Res.* **2020**, *177*, No. 115770.
- (5) Ding, T.; Zhou, Y.; Ong, W. L.; Ho, G. W. Hybrid solar-driven interfacial evaporation systems: beyond water production towards high solar energy utilization. *Mater. Today* **2021**, *42*, 178–191.
- (6) Tao, P.; Ni, G.; Song, C.; Shang, W.; Wu, J.; Zhu, J.; Chen, G.; Deng, T. Solar-driven interfacial evaporation. *Nat. Energy* **2018**, *3*, 1031–1041.
- (7) Zang, L.; Finnerty, C.; Zheng, S.; Conway, K.; Sun, L.; Ma, J.; Mi, B. Interfacial solar vapor generation for desalination and brine treatment: evaluating current strategies of solving scaling. *Water Res.* **2021**, *198*, No. 117135.
- (8) Dao, V. D.; Vu, N. H.; Yun, S. Recent advances and challenges for solar-driven water evaporation system toward applications. *Nano Energy* **2020**, *68*, No. 104324.
- (9) Xu, T.; Xu, Y.; Wang, J.; Lu, H.; Liu, W.; Wang, J. Sustainable self-cleaning evaporator for long-term solar desalination using gradient structure tailored hydrogel. *Chem. Eng. J.* **2021**, *415*, No. 128893.
- (10) Wang, W.; Shi, Y.; Zhang, C.; Hong, S.; Shi, L.; Chang, J.; Li, R.; Jin, Y.; Ong, C.; Zhuo, S.; Wang, P. Simultaneous production of

fresh water and electricity via multistage solar photovoltaic membrane distillation. *Nat. Commun.* **2019**, *10*, 3012.

(11) Zhang, C.; Shi, Y.; Shi, L.; Li, H.; Li, R.; Hong, S.; Zhuo, S.; Zhang, T.; Wang, P. Designing a next generation solar crystallizer for real seawater brine treatment with zero liquid discharge. *Nat. Commun.* **2021**, *12*, 998.

(12) Wang, J.; Li, Y.; Deng, L.; Wei, N.; Weng, Y.; Dong, S.; Qi, D.; Qiu, J.; Chen, X.; Wu, T. High-performance photothermal conversion of narrow-bandgap Ti₂O₃ nanoparticles. *Adv. Mater.* **2017**, *29*, No. 1603730.

(13) Gao, M.; Zhu, L.; Peh, C. K.; Ho, G. W. Solar absorber material and system designs for photothermal water vaporization towards clean water and energy production. *Energy Environ. Sci.* **2019**, *12*, 841–864.

(14) Han, X.; Besteiro, L. V.; Koh, C. S. L.; Lee, H. K.; Phang, I. Y.; Phan-Quang, G. C.; Ng, J. Y.; Sim, H. Y. F.; Lay, C. L.; Govorov, A.; Ling, X. Y. Intensifying heat using MOF-isolated graphene for solar-driven seawater desalination at 98% solar-to-thermal efficiency. *Adv. Funct. Mater.* **2021**, *31*, No. 2008904.

(15) Ma, Q.; Yin, P.; Zhao, M.; Luo, Z.; Huang, Y.; He, Q.; Yu, Y.; Liu, Z.; Hu, Z.; Chen, B.; Zhang, H. MOF-based hierarchical structures for solar-thermal clean water production. *Adv. Mater.* **2019**, *31*, No. 1808249.

(16) Xu, Y.; Tang, C.; Ma, J.; Liu, D.; Qi, D.; You, S.; Cui, F.; Wei, Y.; Wang, W. Low-tortuosity water microchannels boosting energy utilization for high water flux solar distillation. *Environ. Sci. Technol.* **2020**, *54*, 5150–5158.

(17) Zhou, J.; Gu, Y.; Liu, P.; Wang, P.; Miao, L.; Liu, J.; Wei, A.; Mu, X.; Li, J.; Zhu, J. Development and evolution of the system structure for highly efficient solar steam generation from zero to three dimensions. *Adv. Funct. Mater.* **2019**, *29*, No. 1903255.

(18) Wang, P. Emerging investigator series: the rise of nano-enabled photothermal materials for water evaporation and clean water production by sunlight. *Environ. Sci.: Nano* **2018**, *5*, 1078–1089.

(19) Chen, R.; Zhang, T.; Kim, J.; Peng, H.; Ye, M.; Huang, C. H. Interfacial solar distillation for freshwater production: fate of volatile and semivolatile organic contaminants. *Environ. Sci. Technol.* **2021**, *55*, 6248–6256.

(20) Qi, D.; Liu, Y.; Liu, Y.; Liu, Z.; Luo, Y.; Xu, H.; Zhou, X.; Zhang, J.; Yang, H.; Wang, W.; Chen, X. Polymeric membranes with selective solution-diffusion for intercepting volatile organic compounds during solar-driven water remediation. *Adv. Mater.* **2020**, *32*, No. e2004401.

(21) Shi, L.; Shi, Y.; Zhuo, S.; Zhang, C.; Aldrees, Y.; Aleid, S.; Wang, P. Multi-functional 3D honeycomb ceramic plate for clean water production by heterogeneous photo-Fenton reaction and solar-driven water evaporation. *Nano Energy* **2019**, *60*, 222–230.

(22) Zuo, S.; Xia, D.; Guan, Z.; Yang, F.; Cheng, S.; Xu, H.; Wan, R.; Li, D.; Liu, M. Dual-functional CuO/CN for highly efficient solar evaporation and water purification. *Sep. Purif. Technol.* **2021**, *254*, No. 117611.

(23) Ma, X.; Deng, Z.; Li, Z.; Chen, D.; Wan, X.; Wang, X.; Peng, X. A photothermal and Fenton active MOF-based membrane for high-efficiency solar water evaporation and clean water production. *J. Mater. Chem. A* **2020**, *8*, 22728–22735.

(24) Deng, J.; Xiao, S.; Wang, B.; Li, Q.; Li, G.; Zhang, D.; Li, H. Self-suspended photothermal microreactor for water desalination and integrated volatile organic compound removal. *ACS Appl. Mater. Interfaces* **2020**, *12*, 51537–51545.

(25) Song, C.; Qi, D.; Han, Y.; Xu, Y.; Xu, H.; You, S.; Wang, W.; Wang, C.; Wei, Y.; Ma, J. Volatile-organic-compound-intercepting solar distillation enabled by a photothermal/photocatalytic nanofibrous membrane with dual-scale pores. *Environ. Sci. Technol.* **2020**, *54*, 9025–9033.

(26) Oh, W. D.; Dong, Z.; Lim, T. T. Generation of sulfate radical through heterogeneous catalysis for organic contaminants removal: current development, challenges and prospects. *Appl. Catal., B* **2016**, *194*, 169–201.

(27) Teng, Z.; Zhang, Q.; Yang, H.; Kato, K.; Yang, W.; Lu, Y.-R.; Liu, S.; Wang, C.; Yamakata, A.; Su, C.; Liu, B.; Ohno, T. Atomically

dispersed antimony on carbon nitride for the artificial photosynthesis of hydrogen peroxide. *Nat. Catal.* **2021**, *4*, 374–384.

(28) He, X.; Shang, H.; Wang, C.; Chen, L.; Gong, Z.; Wang, J.; Zhao, S.; Ma, J. Significantly influenced photocatalytic performance for H₂O₂ generation over ultrathin g-C₃N₄ through regulating the migration orientation of photogenerated charge carriers. *Chin. Chem. Lett.* **2021**, *32*, 3377–3381.

(29) Tomita, O.; Otsubo, T.; Higashi, M.; Ohtani, B.; Abe, R. Partial oxidation of alcohols on visible-light-responsive WO₃ photocatalysts loaded with palladium oxide cocatalyst. *ACS Catal.* **2016**, *6*, 1134–1144.

(30) Li, H.; Shang, J.; Yang, Z.; Shen, W.; Ai, Z.; Zhang, L. Oxygen vacancy associated surface Fenton chemistry: surface structure dependent hydroxyl radicals generation and substrate dependent reactivity. *Environ. Sci. Technol.* **2017**, *51*, 5685–5694.

(31) Chen, N.; Huang, Y.; Hou, X.; Ai, Z.; Zhang, L. Photochemistry of hydrochar: reactive oxygen species generation and sulfadimidine degradation. *Environ. Sci. Technol.* **2017**, *51*, 11278–11287.

(32) Kim, H.; Lim, J.; Lee, S.; Kim, H. H.; Lee, C.; Lee, J.; Choi, W. Spontaneous generation of H₂O₂ and hydroxyl radical through O₂ reduction on copper phosphide under ambient aqueous condition. *Environ. Sci. Technol.* **2019**, *53*, 2918–2925.

(33) Yu, H. H.; Yan, L. J.; Shen, Y. C.; Chen, S. Y.; Li, H. N.; Yang, J.; Xu, Z. K. Janus poly(vinylidene fluoride) membranes with penetrative pores for photothermal desalination. *Research* **2020**, *2020*, No. 3241758.

(34) Lin, S.; Liu, L.; Liang, Y.; Cui, W.; Zhang, Z. Oil-in-water self-assembled synthesis of Ag@AgCl nano-particles on flower-like Bi₂O₃/CO₃ with enhanced visible-light-driven photocatalytic activity. *Materials* **2016**, *9*, 486.

(35) Liu, Q.; Zeng, C.; Ai, L.; Hao, Z.; Jiang, J. Boosting visible light photoreactivity of photoactive metal-organic framework: designed plasmonic Z-scheme Ag/AgCl@MIL-53-Fe. *Appl. Catal., B* **2018**, *224*, 38–45.

(36) Goetz, S.; Bauch, M.; Dimopoulos, T.; Trassl, S. Ultrathin sputter-deposited plasmonic silver nanostructures. *Nanoscale Adv.* **2020**, *2*, 869–877.

(37) Haag, W. R.; Yao, C. D. Rate constants for reaction of hydroxyl radicals with several drinking water contaminants. *Environ. Sci. Technol.* **1992**, *26*, 1005–1013.

(38) Li, M.; Ramachandran, R.; Sakthivel, T.; Wang, F.; Xu, Z.-X. Siloxene: an advanced metal-free catalyst for efficient photocatalytic reduction of aqueous Cr(VI) under visible light. *Chem. Eng. J.* **2021**, *421*, No. 129728.

(39) Pan, X.; Ji, J.; Zhang, N.; Xing, M. Research progress of graphene-based nanomaterials for the environmental remediation. *Chin. Chem. Lett.* **2020**, *31*, 1462–1473.

(40) Ren, Y.; Liu, Y.; Liu, F.; Li, F.; Shen, C.; Wu, Z. Extremely efficient electro-Fenton-like Sb(III) detoxification using nanoscale Ti-Ce binary oxide: an effective design to boost catalytic activity via non-radical pathway. *Chin. Chem. Lett.* **2021**, *32*, 2519–2523.

(41) Zhou, W.; Cao, M.; Li, N.; Su, S.; Zhao, X.; Wang, J.; Li, X.; Hu, C. Ag@AgHPW as a plasmonic catalyst for visible-light photocatalytic degradation of environmentally harmful organic pollutants. *Mater. Res. Bull.* **2013**, *48*, 2308–2316.

(42) Zhang, Q.; Cobley, C. M.; Zeng, J.; Wen, L. P.; Chen, J. Y.; Xia, Y. N. Dissolving Ag from Au-Ag alloy nanoboxes with H₂O₂: a method for both tailoring the optical properties and measuring the H₂O₂ concentration. *J. Phys. Chem. C* **2010**, *114*, 6396–6400.

(43) Kuang, Y.; Chen, C.; He, S.; Hitz, E. M.; Wang, Y.; Gan, W.; Mi, R.; Hu, L. A high-performance self-regenerating solar evaporator for continuous water desalination. *Adv. Mater.* **2019**, *31*, No. 1900498.

(44) Konstantinou, I.; Albanis, T. TiO₂-assisted photocatalytic degradation of azo dyes in aqueous solution: kinetic and mechanistic investigations. *Appl. Catal., B* **2004**, *49*, 1–14.

(45) Neta, P.; Hoffman, M. Z.; Simic, M. Electron spin resonance and pulse radiolysis studies of the reactions of OH and O⁻ radicals with aromatic and olefinic compounds. *J. Phys. Chem.* **1972**, *76*, 847–853.